applied sciences

MDPI

Article

Design of Multi-Functional Transmitarray with Active Linear Polarization Conversion and Beam Steering Capabilities

In-Gon Lee [1], Jong-Yeong Kim [1] and Ic-Pyo Hong [2,*]

[1] The Specific Radar Team, Hanwha Systems, Yongin 17121, Korea; ig.lee@hanwha.com (I.-G.L.); icejong41@hanwha.com (J.-Y.K.)
[2] Department of Information & Communication Engineering, Kongju National University, Cheonan 31080, Korea
* Correspondence: iphong@kongju.ac.kr; Tel.: +82-41-521-9199

Abstract: This study designed a multi-functional reconfigurable transmitarray with switchable polarization and beam steering capabilities using only a PIN diode having ON/OFF switching ability. The simulation confirmed that the proposed architecture is capable of 2D beam scanning of up to $\pm 45^{\circ}$ for elevation and azimuth while maintaining or converting linear polarization when operating within the X-band. The performance was verified through a far-field beam pattern measurement using the near-field antenna measurement system by producing a transmitarray with an 8×8 unit cell arrangement. The maximum level of gain of the proposed architecture was confirmed to be 14.5 dBi, the sidelobe level was below 14.5 dBc, the polarization converting loss was below 1.28 dB, and the polarization isolation level was above 14.7 dB. It can be utilized for the design technique of a radar system demanding small size, weight, power, and cost (SWaP-C) characteristics based on a simplified composition.

Keywords: transmitarray; switchable polarization; beam steering; SWaP-C

check for updates

Citation: Lee, I.-G.; Kim, J.-Y.; Hong, I.-P. Design of Multi-Functional Transmitarray with Active Linear Polarization Conversion and Beam Steering Capabilities. *Appl. Sci.* **2022**, *12*, 4319. https://doi.org/10.3390/app12094319

Academic Editor: Edik U. Rafailov

Received: 8 April 2022
Accepted: 22 April 2022
Published: 25 April 2022

Publisher's Note: MDPI stays neutral with regard to jurisdictional claims in published maps and institutional affiliations.

Copyright: © 2022 by the authors. Licensee MDPI, Basel, Switzerland. This article is an open access article distributed under the terms and conditions of the Creative Commons Attribution (CC BY) license (https://creativecommons.org/licenses/by/4.0/).

1. Introduction

The transmitarray design technique is actively studied based on the advantage of allowing various functions such as focusing, splitting, and multi-beam generating an electromagnetic (EM) wave emitted from a source antenna or controlling linear and circular polarization without a complex power distribution network when located at the front of a passive legacy antenna [1].

An EM structure commonly used to enable such functionality is a technique of controlling a frequency response attribute by including active elements such as the electromagnetically controllable PIN, varactor diode, or microelectromechanical systems (MEMES) in a periodic configuration that resonates at a specific frequency such as a reconfigurable frequency selective surfaces (FSS) structure [2–4] and reconfigurable metamaterials (MM) [5–10].

As a part of research to develop a high-speed, stable wireless communication technology in a high-density, complex communication environment, the core technology of a point-to-point communication system that can minimize the effect of interference from multipath or a heterogeneous device by tracking and relaying signals to a user or an object from a base-station was developed for application in private sectors [11–13]; separate research on a design technique for a low SWaP-C radar for air or ground surveillance or unmanned aerial vehicles (UAV) continues to be applied in the defense sector [14].

Multi-functional reconfigurable transmitarray was implemented in this study by periodically arranging the reconstruction of a unit cell's frequency response characteristics using the 1-bit ON/OFF switch attributes of the PIN diode. Reconfigurable transmitarray, based on an active element that can be electromagnetically controlled, can be classified into two methods. The first is switching the polarization from vertical to vertical or vertical to horizontal by controlling the direction of the electric current by including the periodic

configuration of a unit cell with a frequency-selective penetration characteristic of an active element [8] or creating a high-gain beam pattern and beam steering function by controlling the path length of an induced current using a variable capacitor [2–5,7,13]. The second is a design method that collects the external incidence of an EM wave through a patch arranged in a periodic configuration and makes the beam steering and polarization conversion (PC) function possible by controlling the phase and direction of the directed electric current which is then reemitted [12,14–21].

Because of the design that includes active elements that directly affect the characteristic impedance of periodically arranged unit cells, the former method facilitates an intuitive design with a relatively simple configuration, which has the advantage of realizing the low-loss reconstruction characteristics. However, there is a disadvantage in that a multi-layer structure of five or more layers is required to secure the broadband response in consideration of the resonance frequency change that varies according to the value.

The latter is a method of reconstructing the EM characteristics via the unit cell's periodic arrangement with a receiver patch–active circuitry–transmitter patch construction and has the benefit of realizing a multi-function based on a stable frequency characteristic by introducing a phase shifter circuitry for the beam shifting functionality or polarization switching circuitry into the part of active circuitry. In addition to the increased design complexity, phase shifter circuitry is limited in that a sufficient area or number of unit cell layers must be secured to realize a wide dynamic range of the available phase-shifting range while suppressing parasitic resonance [18,22].

This study proposes a unit cell design with linear polarization conversion characteristics with a beam steering functionality, capable of turning to the desired direction, and using only a PIN diode to create a reconfigurable multi-function X-band transmitarray. In contrast to other studies, we verified the performance by fabricated finite transmitarray which has a complicated bias network to electrically control [16,17], and to reduce the side effects of the bias network, the decoupling components were designed and presented.

As shown in Figure 1, circular patches including two PIN diodes are located on each of the upper and bottom sides of the ground plane located in the unit cell center. It is configured in the form of a short circuit through a via hole, and multi-functionality is achieved by controlling the current path directed through the receiver unit patch on the bottom side.

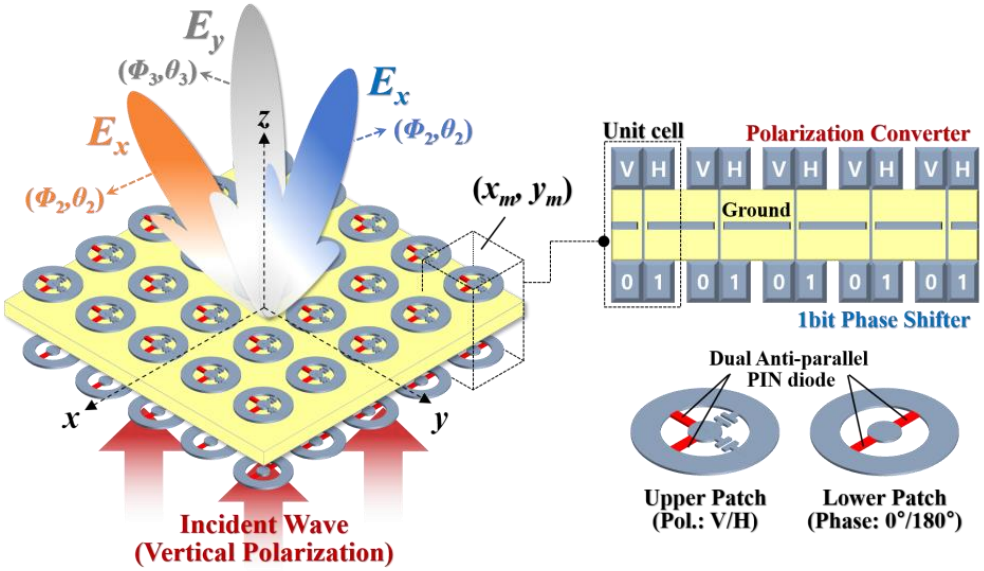


Figure 1. Conceptual schematic view of the proposed multi-functional transmitarray.

This paper consists of five sections. Section 2 explains the beam steering performance estimation of the reconfigurable transmitarray designed based on a PIN diode. In Section 3,

the unit cell with multi-functionality is designed, and its performance result is evaluated and presented using a numerical method and commercial EM field analysis software.

Section 4 takes this design, arranges the unit cells in an 8 × 8, and analyzes the radiation pattern characteristics using a near-field antenna measurement system. Finally, Section 5 concludes the paper.

2. Numerical Analysis of Beam-Steering Performance Based on 1-Bit Quantization

This study presented a design based on 1-bit control to simplify the configuration and implement a multi-function transmitarray, which is different from the previously suggested reconfigurable transmitarray design. Equation (1) shows the calculation of the phase delay characteristics of each unit cell's position ($\vec{r}_{mn}$) deduced from the relationship between the phase ψ_{mn}^{inc}, the source phase ψ_s, and the desired beam steering direction ($\hat{r}_o$), and developed the beam steering characteristics by reconfiguring the phase distribution through electrical control when an EM wave incident from the outside reaches the transmitarray. Here, R_{mn} and k represent each distance from the propagation constant and the source.

$$\psi_{mn}^{tr} = k\left(R_{mn} - \vec{r}_{mn} \cdot \hat{r}_o\right) + \psi_{mn}^{inc} + \psi_s \tag{1}$$

The phase control ability of the unit cell results in quantization loss and therefore affects the efficiency of the transmitarray and the beam steering performance. The beam steering angle range, control margin of error, and efficiency were analyzed to estimate the beam steering performance of the transmitarray created using only a PIN diode having ON/OFF switching characteristics.

Before analyzing the beam steering margin of error, an 8 × 8 transmitarray in which unit cells are arranged at a half-wavelength period of the operating frequency was assumed to configure a focal distance (F/D, ratio of the focal distance F to the aperture size D) carrying the optimal feeding efficiency, and total efficiency was calculated according to the quantization level, the results of which are presented in Table 1. The spillover (η_s), illumination (η_i), and total efficiency ($\eta_t = \eta_s + \eta_i$) can be calculated by the approximation method for aperture efficiency as follows [23] (Equations (2)–(4)). To calculate the radiation pattern of transmitarray, the aperture field can be expressed by (2), where the $\cos^{q_f}$ is feed power pattern, q_f is the feed pattern power factor, θ_f is the angle between source and (m,n)th element, $\vec{r}_f$ is the position vector of the feed, $|T_{mn}|$ is the transmission magnitude of the (m,n)th element, A_p is aperture area, and T is the total number of elements.

$$I_i \approx \frac{\cos^{q_f}\left(\theta_f(m,n)\right)}{\left|\vec{r}_{mn} - \vec{r}_f\right|} \cdot e^{-jk|\vec{r}_{mn} - \vec{r}_f|} \cdot |T_{mn}| e^{j\psi_{mn}^{tr}} \tag{2}$$

$$\eta_s = \frac{2q_f + 1}{2\pi} \sum_{m=1}^{M} \sum_{n=1}^{N} \frac{F \cos^{2q_f}\left(\theta_f\right)}{\left|\vec{r}\right|^3} \Delta x \Delta y \tag{3}$$

$$\eta_i = \frac{1}{A_p} \frac{\left[\int_S I_i dS\right]^2}{\left[\int_S |I_i| dS\right]^2} = \frac{1}{A_p} \frac{\left|\sum_{i=1}^{T} I_i \Delta x \Delta y\right|^2}{\sum_{i=1}^{T} |I_i|^2 \Delta x \Delta y} \tag{4}$$

Table 1. Total efficiency of transmitarray in variation of quantization level.

Classifications	Quantization Level			
	Ideal	**1-bit**	**2-bit**	**3-bit**
Spillover Loss, η_s [dB]	0.48	0.36	0.28	0.53
Illumination Loss, η_i [dB]	0.61	3.65	1.51	0.76
Total Loss, $\eta_t = \eta_s + \eta_i$ [dB]	1.09	4.01	1.79	1.30
Optimum F/D	0.69	0.64	0.60	0.71

Additionally, the beam steering margin of error was analyzed according to the transmitarray's quantization level under the condition of the optimal focal distance, and the results are shown in Figure 2. The calculation confirms that the maximum efficiency decreases as the quantization level decreases, and a maximum of 1.5 degrees of beam steering error is observed within the desired steering range of 0 to 45 degrees and 2.9 dB of quantization loss compared to an optimal condition when a transmitarray unit cell carries a phase control characteristic of 1-bit. The design complexity and cost of the transmitarray were lowered using a low level of quantization to be used in high-security areas and facilities such as border security and a reconnaissance such as land vehicles or UAVs. The loss of efficiency and beam steering error due to design can be compensated by adjusting the aperture size and the number of unit cell arrangements according to the install environment [11,24].

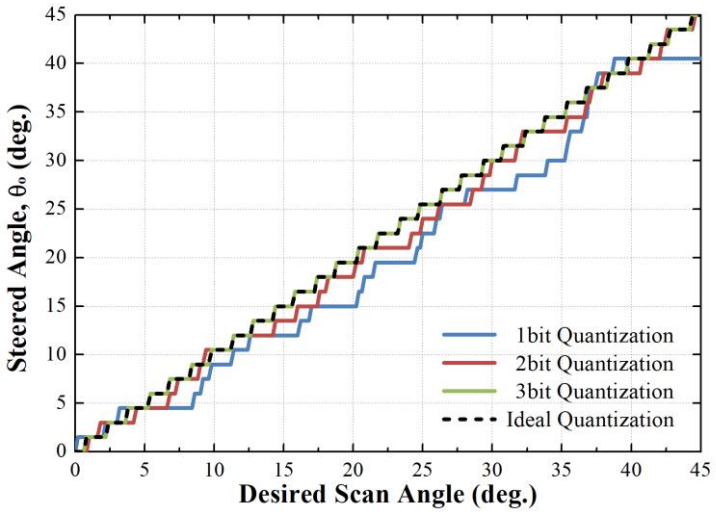


Figure 2. Analysis results of beam scanning error in variation of quantization levels.

3. Design and Simulation of Multi-Functional Transmitarray

The proposed configuration develops 1-bit phase shift characteristics and linear polarization switching functionality by controlling the electrical current path directed to the arranged unit cells. As shown in Figure 3, the configuration of the unit cell on the basis of the ground plane in the center of the circuit board has a circular patch on the bottom side for receiving EM waves from the outside and another circular patch on the top side for re-radiation. Simultaneously, it acts similar to a band-pass filter through an electrically short-circuited configuration through a via hole located in the unit cell center.

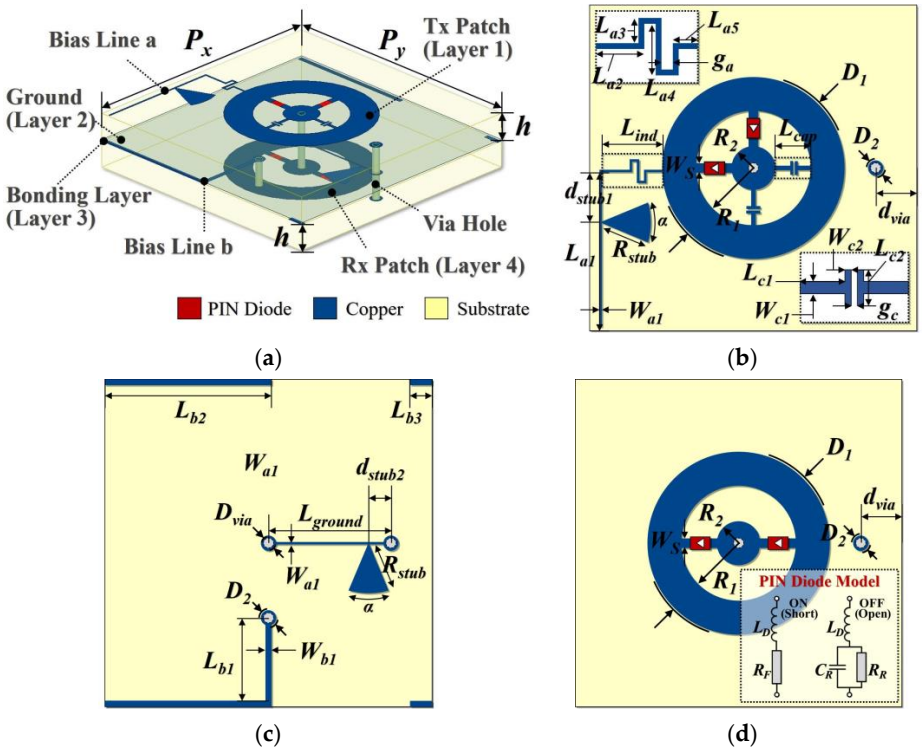


Figure 3. Geometry of proposed unit-cell to implement multi-function: (**a**) Perspective view; (**b**) Tx patch (layer 1); (**c**) Bias line (layer 3, layer 2 is ground plane); (**d**) Rx patch (layer 4).

It was designed to have phase shift characteristics of 0° and 180° through different electrical lengths according to the direction of bias by configuring the circular patch on the bottom side in anti-parallel form using two PIN diodes [25]. The active polarization conversion characteristic was made possible by rotating the direction of the current induced through the circular patch located on the bottom side through two diodes placed on the top side by 90 degrees [26]. A capacitive stub was inserted to mitigate the impedance mismatch caused by an asymmetrical configuration, and an inductive strip line was applied for diode control to ensure isolation from the bias line.

The main design variables that affect the unit cell frequency response characteristic are the diameter of the circular patches on the top and bottom side (D_1), the radius of the circular slot inside the patch (R_1), the diameter of the via hole (D_{via}), and the width of the strip line connecting to the center via hole (W_{S}). The circular patch diameter D_1 and the inner slot radius R_1 determine the operating frequency, and the via hole diameter D_{via} and the strip line connecting to via hole W_{S} affect the unit cell's insert and return loss, thus having a significant effect on impedance matching.

Radial stubs were inserted in each of the polarization control bias (Bias Line **a**) and phase shift bias (Bias Line **b**) to minimize the effect of the bias line needed for diode electrical control, and the optimal variable of the radial angle (α), length (R_{stub}), and position (d_{stub1}, d_{stub2}) were obtained through parametric study to minimize the line's effect on the unit cell frequency characteristic. The proposed configuration is a Taconic RF-35 ($\varepsilon_{\mathrm{r}} = 3.5$, $\tan\delta = 0.0018$, $h = 1.54$ mm) circuit board laminated to a bonding sheet ($\varepsilon_{\mathrm{r}} = 3.26$, $\tan\delta = 0.0025$, $h = 0.1$ mm). The optimized design variable is as follows: $P_{\mathrm{x}} = P_{\mathrm{y}} = 15$ mm, $D_1 = 8.3$ mm, $D_2 = 0.7$ mm, $R_1 = 2.6$ mm, $R_2 = 1.0$ mm, $W_{\mathrm{S}} = 0.4$ mm, $d_{\mathrm{via}} = 1.9$ mm, $L_{\mathrm{ind}} = 2.85$ mm, $L_{\mathrm{a1}} = 7.3$ mm, $L_{\mathrm{a2}} = 1.5$ mm, $L_{\mathrm{a3}} = 0.5$ mm, $L_{\mathrm{a4}} = 1.0$ mm, $L_{\mathrm{a5}} = 0.85$ mm, $g_{\mathrm{a}} = 0.2$ mm, $W_{\mathrm{a1}} = 0.1$ mm, $L_{\mathrm{cap}} = 1.6$ mm, $L_{\mathrm{c1}} = 0.7$ mm, $L_{\mathrm{c2}} = 0.6$ mm, $W_{\mathrm{c1}} = 0.2$ mm, $W_{\mathrm{c2}} = 0.1$ mm, $g_{\mathrm{c}} = 0.1$ mm, $d_{\mathrm{stub1}} = 2.3$ mm, $R_{\mathrm{stub}} = 2.4$ mm, $\alpha = 45°$, $D_{\mathrm{via}} = 0.4$ mm, $L_{\mathrm{b1}} = 4.2$ mm, $L_{\mathrm{b2}} = 7.6$ mm, $L_{\mathrm{b3}} = 0.985$ mm, $L_{\mathrm{ground}} = 5.6$ mm, $W_{\mathrm{b1}} = 0.2$ mm, $d_{\mathrm{stub2}} = 1.0$ mm. The design variable for equivalent circuit modeling of the PIN diode (MACOM MA4GP907) is as follows: $L_{\mathrm{D}} = 0.05$ nH, $R_{\mathrm{F}} = 2.1\ \Omega$, $C_{\mathrm{R}} = 50$ fF, $R_{\mathrm{R}} = 300$ kΩ.

Floquet Mode simulation assuming a periodic structure with an infinitely arranged unit cell was performed using HFSS, a commercial EM field analysis software made by ANSYS, to confirm the frequency response characteristics according to the change in the state of the diode of the designed unit cell.

Figure 4 and Table 2 show the frequency responses for insertion, return loss, phase and isolation level between polarizations at interest frequency band. From the infinite simulation results, the proposed structure has a maximum insertion loss of around 1.29 dB despite the changes of states for the PIN diode, and the isolation level is below 15.7 dB. Moreover, these performances were valid during the phase-shifting operation.

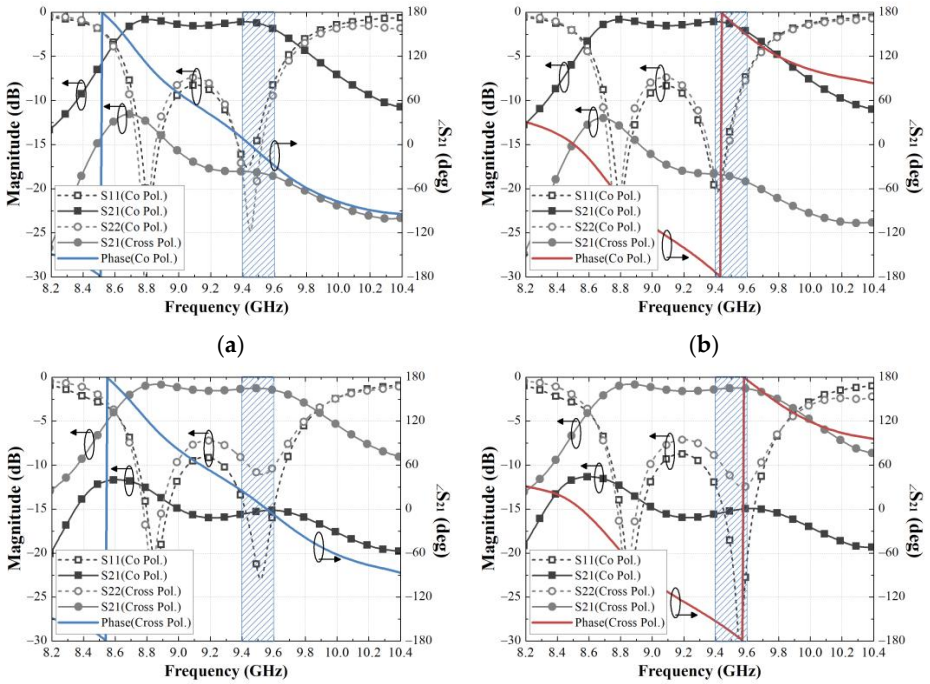


Figure 4. Simulated performance of the proposed unit-cell with changes of diode state: (**a**) State 1 (Pol.: V, Phase: 0°); (**b**) State 2 (Pol.: V, Phase: 180°); (**c**) State 3 (Pol.: H, Phase: 0°); (**d**) State 4 (Pol.: H, Phase: 180°).

Table 2. Simulated performance of the proposed unit-cell (Freq. at Min. insertion loss).

Polarization Conversion	1-bit Phase Shift	Insertion Loss (S_{21}) [dB]	Reflection Loss (S_{11}/S_{22}) [dB]	Cross pol. Level (Isolation) [dB]	Relative Phase (S_{21}) [Deg.]
OFF	OFF	1.13	16.7/24.3	18.1	0
OFF	ON	1.18	16.6/17.8	18.5	177.5
ON	OFF	1.27	18.2/10.4	15.4	−15.5
ON	ON	1.29	15.7/10.4	15.3	167.3

In order to verify the polarization conversion and beam steering performance of a transmitarray arranged with unit cells arranged in a finite number, an 8 × 8 transmitarray arrangement was modeled as shown in Figure 5a, whereas the full-structure simulation for the space feed source was performed using a 10 dBi X-band horn antenna. Cross-validation was performed by comparing the HFSS simulation results and numerical analysis results, which are shown in Figure 5b,d.

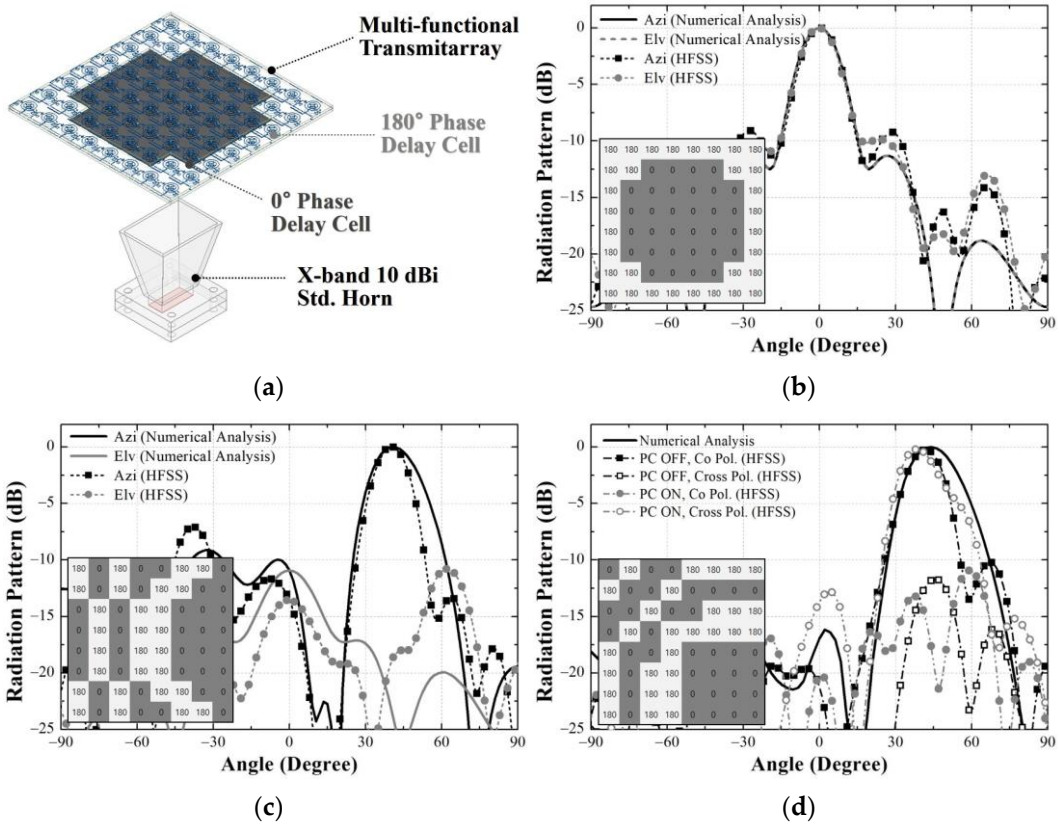


Figure 5. Simulated results of proposed 8 × 8 transmitarray (F/D = 0.64): (**a**) Simulation model (HFSS); (**b**) Broadside beam (V Pol.); (**c**) 45° steered beam with PC OFF state (φ = 0°); (**d**) 45° steered beam (φ = 45°) under the ON and OFF state of PC.

The simulation confirms that beam steering of 0 to 45 degrees and the polarization conversion functionality work as intended on the proposed transmitarray (Figure 5d).

4. Fabrication and Evaluation of Multi-Functional Transmitarray

Based on the results of the simulations performed above, a transmitarray of a size of 120 mm × 120 mm with an 8 × 8 unit cell arrangement was fabricated, and an interface board for the bias control of each unit cell was configured to verify the performance of the proposed structure.

Prior to experiment, an antenna horn with identical specifications from the above simulations was used, and the focal distance was set to 96 mm (F/D = 0.8) for maximum efficiency. The appearance of the fabricated PIN diode-based transmitarray is shown in Figure 6a,b, and the environment in which near-field measuring was performed for radiation pattern measurement to assess beam steering performance is illustrated in Figure 6c.

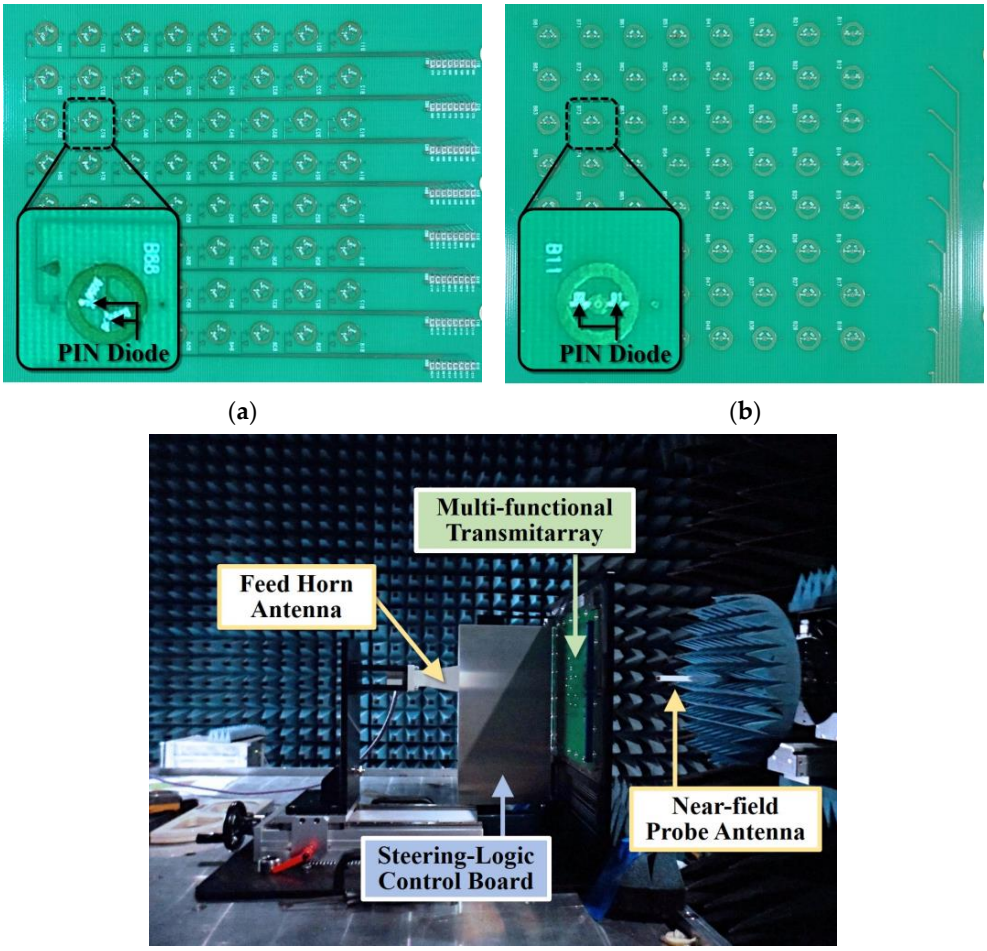


Figure 6. Fabricated 8 × 8 transmitarray: (**a**) top view (Tx patch); (**b**) bottom view (Rx patch); (**c**) far-field pattern measurement based on near-field antenna measurement system.

As demonstrated in Figure 6c, measurement was taken for altering the beam steering angle from 0 to 35 degrees to factor in the physical interference of the support frame that holds the antenna under test (AUT). The 1D beam steer result in comparison to the simulation result is shown in Figure 7a, and the result of the 2D beam steer according to the polarization control status ($\varphi = 30°$, $\theta = 30°$) is shown in Figure 7b.

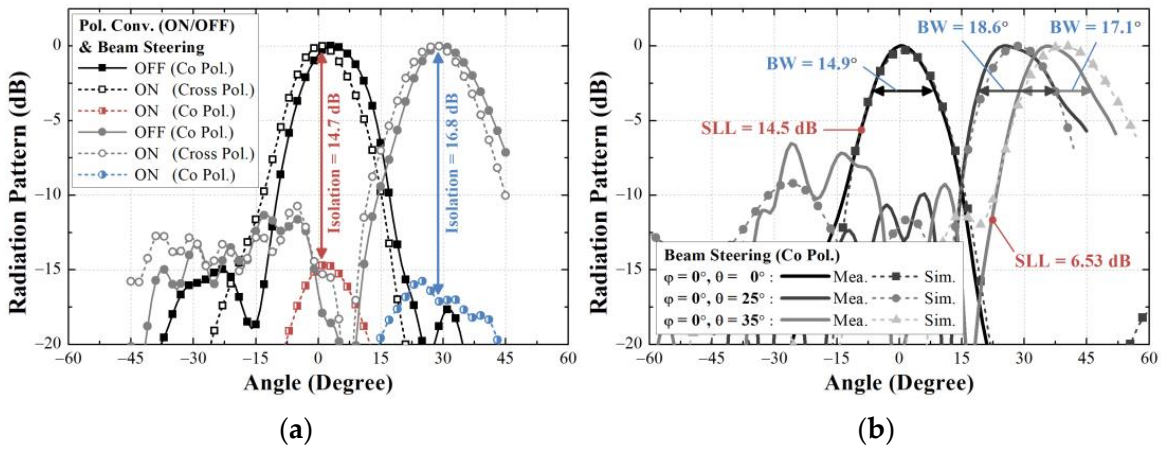


Figure 7. Measured radiation pattern of multi-functional transmitarray. Results of: (**a**) scan angle in horizontal plane; (**b**) scan angle in diagonal planes with the state changes of polarization.

The measured maximum gain was observed to be 14.6 dBi under the condition of the Bore-sight ($\varphi = 0°$, $\theta = 0°$), and the beam width and side lobe level (SLL) are measured as 14.9° and 14.5 dB, respectively. The isolation level between the polarizations under bore-sight conditions is 14.7 dB. It was confirmed that both the polarization conversion and beam steering operate simultaneously without issues.

According to the unit cell simulation and measurement results, the design margin of error is 160 MHz. This is considered because of the photoimageable solder resist (PSR) layer with a permittivity of 3.3 coated on both sides of the circuit board to prevent corrosion of the fabricated transmitarray bare board. Aperture efficiency calculated by the ratio of the measured benefit compared to the maximum directivity of $D_{max} = 4\pi A/\lambda_2 = 22.4$ dBi that can be gained from the aperture area A is 16.4%.

The gain–loss budget, which analyzes any factors contributing to the efficiency loss, is illustrated in Table 3 (where λ is the working frequency). Relatively significant loss due to fabrication and measurement was observed. This may be due to the resolution error over-etching of the copper line and fabrication error caused by the manual mounting of the PIN diode during the build-up process used to produce the transmitarray. These factors are believed to be improved if a high-precision fabrication process is used.

Lastly, a performance comparison of the proposed design result to the previous studies of the transmitarray design based on a PIN diode is summarized as shown in Table 4.

Table 3. Gain loss analysis for boresight beam.

Aperture Size	120 mm × 120 mm
Measured Gain	14.6 dBi
Ideal Directivity	22.4 dBi
Spillover Loss	0.4 dB
Illumination Loss	1.0 dB
1bit Quantization Loss	2.6 dB
Element Insertion Loss	1.3 dB
Reflection and Cross-Polarization Loss	0.6 dB
PIN Failure Loss	0.8 dB
Losses from Fabrication, Assembly and Measurement Errors	1.2 dB

Table 4. Performance comparison with previous similar studies.

Ref.	Phase Resolution	Layers	Size of Unit Cell	Gain [dBi]	Ap. Effi. [%]	Polarization Conversion	Beam Scanning Capability
[4]	1 bit	5	$0.54\lambda \times 0.54\lambda$	21.0 (Sim.)	24.2 (Sim.)	Passive LP	±40° E-, and H-planes
[12]	2 bit	4	$0.49\lambda \times 0.49\lambda$	18.3	9.5	Active CP	±60° E-, and H-planes
[15]	1 bit	4	$0.50\lambda \times 0.50\lambda$	22.8	15.9	N/A	±40° E-, and ±70° H-planes
[16]	1 bit	4	$0.51\lambda \times 0.51\lambda$	N/A	N/A	Active LP	N/A
[17]	1 bit	4	$0.48\lambda \times 0.48\lambda$	N/A	N/A	Active CP	N/A
[19]	1 bit	4	$0.33\lambda \times 0.33\lambda$	17.0	14.0	Passive LP	±50° E-, and H-planes
[20]	2 bit	6	$0.49\lambda \times 0.49\lambda$	19.8	15.9	Passive LP	±60° E-, and H-planes
[21]	1 bit	4	$0.54\lambda \times 0.54\lambda$	21.4	14.7	Passive LP	±60° E-plane
[27]	1 bit	5	$0.29\lambda \times 0.29\lambda$	16.8	18.4	Passive LP	±40° E-, and H-planes
This work	1 bit	4	$0.50\lambda \times 0.50\lambda$	14.6	16.4	Active LP	±45° E-, and H-planes

5. Conclusions

This study designed, fabricated, and verified the performance of a multi-functional transmitarray using only a PIN diode having ON/OFF switching characteristics. The transmitarray was designed based on a minimized level of quantization while reducing the design complexity and cost to be used as a low SWaP-C radar for UAV or air or ground surveillance system. The proposed configuration offers beam steering (1-bit phase resolution) and switchable linear-to-linear polarization characteristics through four PIN diodes in a unit cell. The calculation results confirmed the ability of the 8×8 transmitarray to 2D beam scan on a $90^\circ \times 90^\circ$ area, polarization converting loss of below 1.28 dB, and polarization isolation of over 10 dB. The far-field pattern was measured through near-field antenna measurement system to verify the fabricated transmitarray and maximum gain of 14.6 dBi (Bore-sight), and an aperture efficiency of 16.4% were observed through the measured data showing an improvement in performance compared to previous studies despite demonstrating multi-functionality.

Author Contributions: Conceptualization, I.-G.L. and I.-P.H.; methodology, I.-G.L. and I.-P.H.; investigation, I.-G.L.; validation, I.-G.L. and J.-Y.K.; writing—original draft preparation, I.-G.L.; writing—review and editing, I.-P.H.; supervision, J.-Y.K. and I.-P.H.; project administration, I.-P.H. All authors have read and agreed to the published version of the manuscript.

Funding: This research has been supported by a grant-in-aid of HANWHA SYSTEMS based on the Challenging Future Defense Technology Research and Development Program (9127786) of Agency for Defense Development in 2019.

Institutional Review Board Statement: Not applicable.

Informed Consent Statement: Not applicable.

Data Availability Statement: Not applicable.

Conflicts of Interest: The authors declare no conflict of interest.

References

1. Reis, J.R.; Vala, M.; Caldeirinha, R.F. Review paper on transmitarray antennas. *IEEE Access* **2018**, *7*, 94171–94188. [CrossRef]
2. Pan, W.; Huang, C.; Chen, P.; Pu, M.; Ma, X.; Luo, X. A beam steering horn antenna using active frequency selective surface. *IEEE Trans. Antennas Propag.* **2013**, *61*, 6218–6223. [CrossRef]
3. Reis, J.R.; Copner, N.; Hammoudeh, A.; Al-Daher, Z.M.E.; Caldeirinha, R.F.; Fernandes, T.R.; Gomes, R. FSS-inspired transmitarray for two-dimensional antenna beamsteering. *IEEE Trans. Antennas Propag.* **2016**, *64*, 2197–2206. [CrossRef]
4. Nguyen, B.D.; Pichot, C. Unit-cell loaded with PIN diodes for 1-bit linearly polarized reconfigurable transmitarrays. *IEEE Antennas Wirel. Propag. Lett.* **2018**, *18*, 98–102. [CrossRef]
5. Jiang, T.; Wang, Z.; Li, D.; Pan, J.; Zhang, B.; Huangfu, J.; Ran, L. Low-DC voltage-controlled steering-antenna radome utilizing tunable active metamaterial. *IEEE Trans. Microw. Theory Techn.* **2011**, *60*, 170–178. [CrossRef]
6. Turpin, J.; Werner, P.D.H.; Wolfe, D.E. Design considerations for spatially reconfigurable metamaterials. *IEEE Trans. Antennas Propag.* **2015**, *63*, 3513–3521. [CrossRef]
7. Huang, C.; Zhang, C.; Yang, J.; Sun, B.; Zhao, B.; Luo, X. Reconfigurable metasurface for multifunctional control of electromagnetic waves. *Adv. Opt. Mater.* **2017**, *5*, 1700485. [CrossRef]
8. Li, Y.; Cao, Q.; Wang, Y. A wideband multifunctional multilayer switchable linear polarization metasurface. *IEEE Antennas Wirel. Propag. Lett.* **2018**, *17*, 1314–1318. [CrossRef]
9. Hum, S.V.; Perruisseau-Carrier, J. Reconfigurable reflectarrays and array lenses for dynamic antenna beam control: A review. *IEEE Trans. Antennas Propag.* **2014**, *62*, 183–198. [CrossRef]
10. Lu, L.; Simpson, R.E.; Valiyaveedu, S.K. Active hyperbolic metamaterials: Progress, materials and design. *J. Opt.* **2018**, *20*, 103001. [CrossRef]
11. Wu, Q.; Zhang, R. Beamforming optimization for wireless network aided by intelligent reflecting surface with discrete phase shifts. *IEEE Trans. Commun.* **2020**, *68*, 1838–1851. [CrossRef]
12. Di Palma, L.; Clemente, A.; Dussopt, L.; Sauleau, R.; Potier, P.; Pouliguen, P. Circularly-polarized reconfigurable transmitarray in Ka-band with beam scanning and polarization switching capabilities. *IEEE Trans. Antennas Propag.* **2017**, *65*, 529–540. [CrossRef]
13. Pham, T.K.; Guang, L.; González-Ovejero, D.; Sauleau, R. Dual-band transmitarray with low scan loss for satcom applications. *IEEE Trans. Antennas Propag.* **2021**, *69*, 1775–1780. [CrossRef]
14. Nicholls, J.G.; Hum, S.V. Full-space electronic beam-steering transmitarray with integrated leaky-wave feed. *IEEE Trans. Antennas Propag.* **2016**, *64*, 3410–3422. [CrossRef]

15. Clemente, A.; Dussopt, L.; Sauleau, R.; Potier, P.; Pouliguen, P. Wideband 400-element electronically reconfigurable transmitarray in X band. *IEEE Trans. Antennas Propag.* **2013**, *61*, 5017–5027. [CrossRef]
16. Pan, W.; Huang, C.; Ma, X.; Jiang, B.; Luo, X. A dual linearly polarized transmitarray element with 1-bit phase resolution in X-band. *IEEE Antennas Wirel. Propag. Lett.* **2014**, *14*, 167–170. [CrossRef]
17. Huang, C.; Pan, W.; Ma, X.; Luo, X. 1-bit reconfigurable circularly polarized transmitarray in X-band. *IEEE Antennas Wirel. Propag. Lett.* **2015**, *15*, 448–451. [CrossRef]
18. Huang, C.; Pan, W.; Ma, X.; Zhao, B.; Cui, J.; Luo, X. Using reconfigurable transmitarray to achieve beam-steering and polarization manipulation applications. *IEEE Trans. Antennas Propag.* **2015**, *63*, 4801–4810. [CrossRef]
19. Wang, M.; Xu, S.; Yang, F.; Li, M. Design and measurement of a 1-bit reconfigurable transmitarray with subwavelength H-shaped coupling slot elements. *IEEE Trans. Antennas Propag.* **2019**, *67*, 3500–3504. [CrossRef]
20. Diaby, F.; Clemente, A.; Sauleau, R.; Pham, K.T.; Dussopt, L. 2 bit reconfigurable unit-cell and electronically steerable transmitarray at Ka-band. *IEEE Trans. Antennas Propag.* **2019**, *68*, 5003–5008. [CrossRef]
21. Wang, Y.; Xu, S.; Yang, F.; Li, M. A novel 1 bit wide-angle beam scanning reconfigurable transmitarray antenna using an equivalent magnetic dipole element. *IEEE Trans. Antennas Propag.* **2020**, *68*, 5691–5695. [CrossRef]
22. Tang, J.; Xu, S.; Yang, F.; Li, M. Design and measurement of a reconfigurable transmitarray antenna with compact varactor-based phase shifters. *IEEE Antennas Wirel. Propag. Lett.* **2021**, *20*, 1998–2002. [CrossRef]
23. Abdelrahman, A.H.; Yang, F.; Elsherbeni, A.Z.; Nayeri, P.C.; Balanis, A. *Analysis and Design of Transmitarray Antennas*; Morgan & Claypool: San Francisco, CA, USA, 2017.
24. Yang, H.; Yang, F.; Xu, S.; Li, M.; Cao, X.; Gao, J.; Zheng, Y. A study of phase quantization effects for reconfigurable reflectarray antennas. *IEEE Antennas Wirel. Propag. Lett.* **2016**, *16*, 302–305. [CrossRef]
25. Rana, B.; Lee, I.G.; Hong, I.P. Experimental characterization of 2 $\times$ 2 electronically reconfigurable 1 bit unit cells for a beamforming transmitarray at X band. *J. Electromagn. Eng. Sci.* **2021**, *21*, 153–160. [CrossRef]
26. Rana, B.; Lee, I.G.; Hong, I.P. Experimental characterization of 2 $\times$ 2 electronically reconfigurable polarization converter unit cells at X-Band. *Int. J. Antennas Propag.* **2021**, *2021*, 5536864. [CrossRef]
27. Luo, C.W.; Zhao, G.; Jiao, Y.C.; Chen, G.T.; Yan, Y.D. Wideband 1 bit reconfigurable transmitarray antenna based on polarization rotation element. *IEEE Antennas Wirel. Propag. Lett.* **2021**, *20*, 798–802. [CrossRef]